Eur Biophys J (1998) 27: 595–604

ARTICLE

Olivier Helluin · Saïd Bendahhou · Hervé Duclohier

Voltage sensitivity and conformational change of isolated S4L45 fragments from sodium channels are tuned to proline

Received: 28 October 1997 / Revised version: 4 March 1998 / Accepted: 26 March 1998

Abstract Peptide fragments reproducing the sequences of S4 segments extended with L45 linkers from the four homologous domains of the electric eel sodium channel were chemically synthesized and purified to allow circular dichroism studies in various solvents and conductance assays in planar lipid bilayers. Repeats III (with proline) and IV (lacking proline) present the lowest and highest helicities, respectively. The conformational transition (from helix to β-strand) shown to occur on an increase of solvent dielectric constant is broader with repeat III. Analytical ultracentrifugation (interference fringe pattern) is consistent with a monodispersion of the peptide. In macroscopic conductance experiments, the proline containing peptides (repeats I, II and especially III) display higher voltage-sensitivities than repeat IV. The apparent and averaged number of monomers per intramembrane conducting aggregate is 4–5. The influence of proline is confirmed in similar experiments carried out on homologous S4 segments of repeat IV of the human skeletal muscle sodium channel comparing the wild type and an analogue where the fourth arginine was substituted with a proline. Thus, both conformational switching and voltage-sensitivity appear correlated to the presence and position of a single proline residue. Since voltage sensors are likely to experience different polarity environments in the channel open and closed states, our results suggest an alternative gating mechanism, i.e. a voltage-driven conformational change of S4L45s. The data also implies a plausible functional asymmetry, namely a "three- or four-stroke" activation sequentially involving the four domains of the sodium channel.

Key words Voltage sensors · Gating mechanisms · Synthetic peptides · Planar lipid bilayers · Macroscopic conductances · Circular dichroism · Dielectric constant

O. Helluin · S. Bendahhou[1] · H. Duclohier (✉)
Biopolymères, Polymères, Membranes,
UMR 6522 CNRS-Université de Rouen
(Institut Fédératif de Recherche Multiplidisciplinaire
sur les Peptides, IFR 23),
Boulevard M. de Broglie, F-76821 Mont-Saint-Aignan, France
e-mail:Herve.Duclohier@univ-rouen.fr

O. Helluin
The Johnson Research Foundation
for Molecular Biophysics and Structural Biology,
Department of Biochemistry and Biophysics,
University of Pennsylvania School of Medicine,
Philadelphia, PA 19104-6059, USA

Present address:
[1] "Howard Hughes Medical Institute", Eccles Institute of
Human Genetics, Building 533, University of Utah,
Salt Lake City, UT 84112, USA

Introduction

Within the six transmembrane segments of each homologous domain making up the action potential sodium channel, the highly charged S4 segments have been identified as the main voltage sensors, i.e. elements whose response to transmembrane voltage changes initiate activation, a sequence of events leading to channel opening. The initial hypothesis put forward by Noda et al. (1984) and further elaborated in the first topological models (Greenblatt et al. 1985; Guy and Seetharamulu 1986) has been experimentally confirmed in numerous studies. In particular, Stühmer et al. (1989) showed that serial neutralizations of arginines (occurring every three residues) in S4s of rat brain sodium channel II resulted in progressive reduction of the slope of the activation curve. Some selected neutral residue mutations also shifted activation curves (Auld et al. 1990). These findings were later extended to potassium channels (Lopez et al. 1991; Logothetis et al. 1992; Perozo et al. 1994). Recently, there has been a new surge of interest in S4s with demonstrations of their outward movements or exposure upon depolarization, employing fluorescence-labelling or cysteine modifying reagents on selected key residues mutated to Cys in the *Shaker* K^+ channel (Mannuzzu et al. 1996; Cha and Bezanilla 1997) and in the Na^+ channel (Yang et al. 1996). Neighbouring negatively-charged transmembrane segments S2 and especially S3 shown to

facilitate the proper folding of the channel (Tiwari-Woodruff et al. 1997) are also involved to some extent in the gating process (Planells-Cases et al. 1995; Seoh et al. 1996). It was further shown that the length of the S3–S4 linker in the *Shaker* channel can modulate activation kinetics (Mathur et al. 1997). This linker transferred from the voltage-independent (despite the presence of S4s) rat olfactory cyclic nucleotide-gated channel to a voltage-dependent channel ("ether-a-gogo" K^+ channel) confers voltage-insensitivity to the latter (Tang et al. 1997).

Contrasting with this wealth of functional data, the absence of direct structural information at the level of the whole channel precludes a detailed molecular description of gating. An initial secondary structure study of purified and reconstituted sodium channel employing circular dichroism spectroscopy reported a 65% alpha-helical content (Elmer et al. 1985). Since then, models describing the architecture of the whole channel emerged and specific issues of channel structure-function were addressed (for gating, see e.g. Guy and Conti 1990; Durell and Guy 1992). Molecular modelling simulations are currently developing, especially for the toxin binding sites and selectivity filter of the sodium channel (Lipkind and Fozzard 1994; Favre et al. 1996) and for the somewhat simpler potassium channels (Durell and Guy 1996; Kerr and Sansom 1997). Efforts are also being made towards 2D- and 3D-crystallizations (Li et al. 1994; Spencer et al. 1997; Kreusch et al. 1998).

In the meantime, the "peptide strategy" first applied by Oiki et al. (1988) and Tosteson et al. (1989) was recognized as a plausible alternative (Stühmer 1991). This approach reviewed by Montal (1995, 1996) and Marsh (1995) makes use of the ability of natural peptides or amphipathic segments designed along 'first chemical principles' (DeGrado et al. 1988) to form ion pores in lipid bilayers (for review, see e.g. Sansom 1991). Data can be compared to electrophysiological studies on the whole in situ heterologously expressed channel and interpreted in terms of molecular models. The approach is validated by the finding that isolated segments can adopt similar conformations as in the whole membrane protein, in the few cases where such a comparison can be safely made (e.g. Barsukov et al. 1992). In addition, some synthetic peptides reproducing isolated transmembrane helices of membrane proteins can self-assemble in lipid systems and functional properties of the parent protein can be retrieved (Kahn and Engelman 1992).

In the present study, we compare functional properties (macroscopic conductances in planar lipid bilayers) and conformations (ellipticities as a function of solvent polarity) of the four S4 segments of the electric eel sodium channel extended with L45 linkers, and of the homologous human skeletal muscle S4 (domain IV). Amino acid sequences are shown in Table 1 together with that of a scrambled peptide simply derived by a random selection of residues from the averaged composition of the four eel S4L45s. We show here that both the intrinsic voltage-sensitivity of this family of isolated voltage sensors as assayed in predominantly hydrophobic environments and solvent polarity-dependent secondary structural change are tuned to the presence and position of a single proline.

Table 1 Amino acid sequences of the four homologous S4L45s from the electric eel sodium channel. Positions are from Noda et al. (1984): 207–240, 654–687, 1092–1125, and 1414–1447 for repeats I, II, III and IV, respectively. The extremities of S4L45 (IV) N-deleted fragments are also shown together with a previously studied eel S4 (IV) labelled as T (Tosteson et al. 1989). Homologous S4s from human skeletal muscle isoform (George et al. 1992) are shown for the wild type and R4P substitution. At the bottom of the table is the 'scrambled' or 'control random' peptide. Positively-charged residues are in bold and prolines are shaded and framed. Gaps are introduced between the S4 (*on the left*) and L45 (*on the right*) moieties

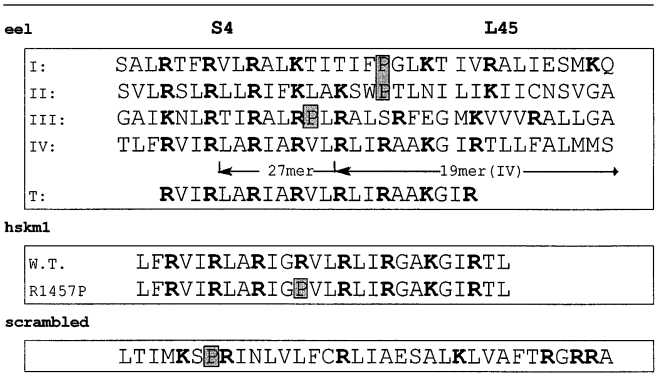

Materials and methods

Solid phase peptide synthesis, purification and characterization

All peptides were synthesized by the Merrifield solid-phase technique (see Atherton and Sheppard 1989). S4L45, fragments and L45 of repeat IV were prepared on a SAP 4 synthesizer (Sempa-Chimie, Paris) and using the *t*-BOC strategy on a benzhydrylamine resin reticulated by 1% divinylbenzene. Boc-aminoacids were obtained from Bachem (Bubendorf, Switzerland) and other reagents included trifluoroacetic acid (Sigma), N,N-diisopropyl-ethylamine (Aldrich), dicyclohexylcarbodiimide (Fluka), 1-hydroxybenzotriazole (Fluka), methylene chloride (Carbo Erba), and dimethyl formamide (Aldrich). To avoid oxidization hazards during subsequent purification, Met residues in the native sequence were replaced by *nor*-Leu. After I24, R16 and L8 had been coupled, aliquots of the peptidyl-resin were put aside before completion of the synthesis. The peptide and its fragments, the first of which (11 residues) corresponding to the L45 linker, were then released from the resin and sidechain protecting groups eliminated by the usual fluorhydric acid treatment. The three other homologous S4L45s, from domains or repeats I to III, supplied by the CEB (Mont-Saint-Aignan, France), were prepared *via* the Fmoc strategy on a 433. A peptide synthesizer (Applied Biosystems, Forster City, CA, USA) with a Rink amide MBHA resin (Novabiochem, Switzerland). As for S4s from domain IV of the human skeletal muscle (hskm1) sodium channel, the wild type analogue was prepared with

similar techniques as above by Dr. M. Beyermann and the R1457P substituted analogue was supplied by Quantum Biotechnologies Inc. (Québec, Canada). The lyophilized raw products were purified by high-performance liquid chromatography (HPLC LKB System, series 2100 from Pharmacia LKB, Bromma, Sweden) on a Nucleosil C18 reverse phase semi-preparative column (10 μm particle, 8×300 mm), from Société Francaise Chromato Colonne/ Shandon Scientific (Eragny, France). The flow rate was 1.5 mL per minute under acetonitrile (HPLC grade, Janssen)/H_2O gradients with 0.1% trifluoroacetic acid. Peptide homogeneity (≥95%) was determined by analytical HPLC also using the above gradients and the peptide contents were determined by amino acid analysis at the "Institut de Biologie Structurale" (Grenoble, France). Molecular weights were checked by MALDI-TOF mass spectrometry at the "Laboratory of Chimie Structurale, Organique et Biologique" (Université Pierre et Marie Curie, Paris).

Circular dichroism spectroscopy (CD)

CD spectra were recorded in steps of 1 nm from peptide solutions (1 mg/mL) in 2-propanol/H_2O in varying proportions using a Jobin-Yvon Dichrograph Mark V (Lonjumeau, France) at room temperature. HPLC grade 2-propanol was purchased from Carlo Erba (Milan, Italy). The instrument had previously been calibrated for peaks and ellipticity values of a standard solution of *d*-camphorsulfonic acid. All ellipticity measurements are reported as mean residue ellipticity [Θ] with the units $\deg \cdot cm^2 \cdot dmol^{-1}$, the mean residue weight being 111 and 116 g/mole for repeat III and IV, respectively. Each spectrum was the average of 5 scans. The sensitivity was set at 5×10^{-6} or 1×10^{-5}, the pathlength at 0.01 cm and the response time constant at 5 s in the range 185 – 260 nm. The different conformational contents were estimated from 51 mean residue ellipticity values (from 190 to 240 nm, every nanometer) and computed using the standards of Chang et al. (1978). The quality of the fit between the calculated ellipticities and the experimental points was estimated from normalized mean root square deviations or NMRSD (Brahms and Brahms 1980). The algorithm for conformational contents was constrained, i.e. the sum of contents was set to 100%.

Analytical ultracentrifugation (interference fringe pattern)

Measurements were made using a Beckman XL-I analytical ultracentrifuge (Furst 1997). Peptide samples were dissolved at 1 mg/ml (300 micromolar) in a mixed 2-propanol/H_2O solvent of known composition. Sedimentation equilibrium experiments were done at 48,000 RPM in six-channel, carbon-epoxy composite centerpieces supplied by Beckman. Equilibrium was assessed by the absence of significant change in radial concentration gradients in scans separated by a few hours. Data were analyzed by curve-fitting to the equation for a single ideal species using Igor-Pro® (Wavemetrics, Lake Oswego, OR) programs developed from a previous version (Brooks et al. 1993).

The equation is:

$$C(r) = C(r_0)\exp\left\{\frac{(1-\bar{\nu}\,\rho)\,\omega^2 M_n}{2RT}(r^2 - r_0^2)\right\}$$

where:

$C(r, r_0)$ = concentration (any units) of sedimenting species at radial positions r, r_0 cm from the center of rotation.
$\bar{\nu}$ = partial specific volume of sedimenting species (cc/gm)
ρ = density of supporting buffer (gms/cc)
ω = angular velocity of rotor (radians/sec)
M_n = "Molar" molecular weight of sedimenting species (gms/mole)
M_b = "Buoyant" molecular weight = $M_n(1-\bar{\nu})$
R = Gas constant (8.35×10^7 ergs $°K^{-1}$ mol^{-1}
T = Temperature (°K)

Peptide partial specific volumes and solvent densities were calulated using the program "Sedinterp" (Laue et al. 1992). We estimate an uncertainty of ±10% in the calculated molecular weight of the protein. This arises largely from uncertainty in the partial specific volume which is calculated from a weight average of individual amino acids. This degree of accuracy is sufficient to distinguish peptide monomers from aggregates. The inclusion of added electrolyte (0.12 M KCl) was done to eliminate polyelectrolyte effects which reduce the apparent molecular weight by a factor of about 1.6 for these highly charged peptides (Braswell 1987).

Peptide reconstitution into planar lipid bilayers: macroscopic conductances

To form virtually solvent-free bilayers (Montal and Mueller 1972), buffer (0.5 M NaCl or KCl, 10 mM HEPES, pH 7.4) was added both sides of a 25 μm thick PTFE septum (Goodfellow, Cambridge, UK) sandwiched between two half glass cells. Lipid monolayers were spread from a 10 mg/mL solution in hexane (spectroscopic grade, Fluka) on top of the electrolyte whose level was above a 150 – 200 μm hole in the septum. A mixture of neutral lipids from Avanti Polar Lipids (Alabater, AL, USA) was used: 1-palmitoyl-2-oleoylphosphatidylcholine (POPC)/ 1,2-dioleoylphosphatidylethanolamine (DOPE), 7/3 (w/w). After 15 minutes of allowing hexane to evaporate, the buffer level on the *trans*-side was lowered below the hole, then raised back to its original level. Planar bilayer formation was monitored through capacitance responses and once typical values were reached, bilayers were submitted to slow triangular voltage waveforms (40 s/period). After checking stability and electrical silence of bare bilayers, peptides from methanol solution (final concentration ≤1%)

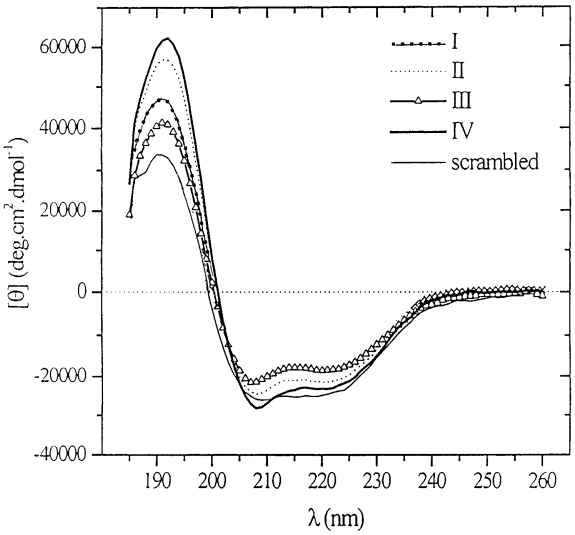

Fig. 1 CD spectra family for the four repeats and the scrambled peptide at 1 mg/mL in 2-propanol/H_2O (75/25, v/v) and room temperature. Five scans averaged in all cases

were added to the *cis*- or positive-side of the chamber. Transmembrane currents were fed to a Keithley amplifier (model 427; Cleveland, OH) virtually-grounded to the *trans* Ag/AgCl electrode (voltages being delivered via the *cis*-electrode). Current-Voltage (I–V) curves were recorded with a X–Y plotter (model Ly 1600, Linseis, Selb, Germany).

Parameters essential for the analysis of macroscopic conductance data are defined as: Ve, the voltage increment producing an e-fold increase in conductance, and Va, the voltage threshold shift – for a given reference conductance, typically 10×(bare membrane conductance) – induced by an e-fold change in peptide bath concentration (see Fig. 4A). As shown earlier for alamethicin and other voltage-dependent channel-forming peptides (Hall et al. 1984), the apparent and mean number of peptide monomers per intramembrane conducting aggregate can then be simply estimated as $\langle N \rangle = Va/Ve$.

Table 2 Secondary structures of the four homologues derived from CD spectra shown in Fig. 1, and of the scrambled peptide, analyzed according to Chang and Yang (1978)

Peptide	Helix (%)	Sheet (%)	Random (%)	NMRSD (%)
S4-L45 (I)	55	10	35	9.0
S4-L45 (II)	60	10	30	9.2
S4-L45 (III)	50	10	40	8.7
S4-L45 (IV)	70	0	30	9.4
Scrambled	55	0	45	18.4

Results

Secondary structures

Comparison of Circular Dichroism (CD) spectra. CD spectra of the four S4L45s recorded under the same conditions and especially in the same solvent mixture (2-propanol/H_2O, 75/25) are compared in Fig. 1. In all cases, CD spectra show the twin negative peaks at around 208 and 222 nm and the positive peak at 192 nm, typical for a predominantly helical structure. Largest peaks are for repeat IV (devoid of Pro) whereas smallest ones are recorded with repeat III (with a Pro at position 14). Conformational contents derived from these spectra are summarized in Table 2. Whereas in 2-propanol/H_2O (75/25; vol/vol) the helicity of repeat IV reaches 70%, it is significantly reduced for the other three segments containing a proline (Table 2), in agreement with the well-known effect of this residue (see e.g. Barlow and Thornton 1988). Data for the scrambled peptide show that it presents the highest tendency of the five peptides to form a random coil. Nevertheless, helicity is still predominant and this is probably because this peptide has its proline near the N-terminus, leaving a long stretch of helix-forming residues.

Conformational contents and oligomerization state as a function of the solvent dielectric constant. Investigation of the conformational contents of the four homologues as a function of the medium polarity (Fig. 2) reveals an $\alpha \rightarrow$

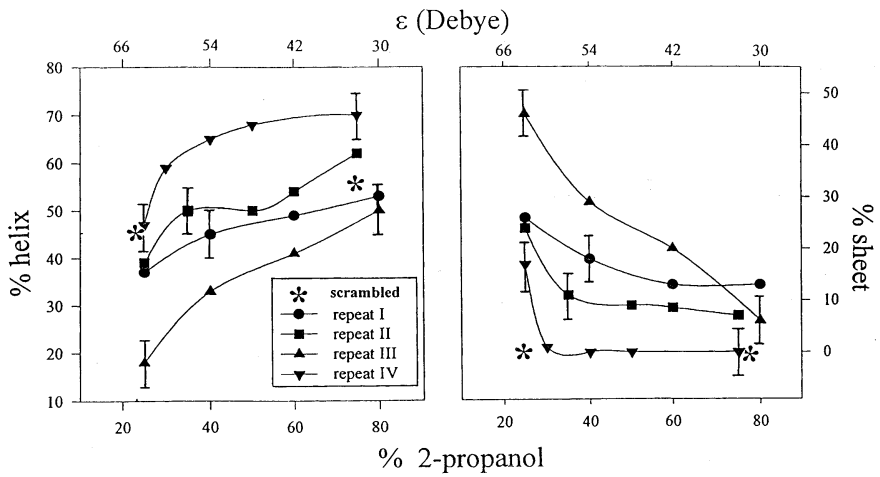

Fig. 2 Conformational contents (α-helix on the left and β-sheet on the right) of the four homologous repeats as a function of 2-propanol percentage and medium dielectric constant. Data for the scrambled peptide at both extrema of ε range are also shown (*bold asterisks*)

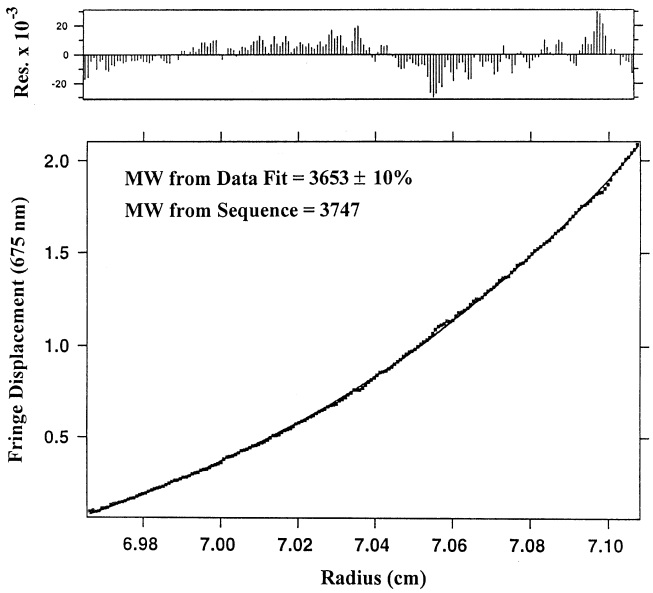

Fig. 3 Sedimentation curve of S4L45 (III) at 1 mg/mL in 67.5% 2-propanol, 0.12 M KCl. $T = 20\,°C$

(β+random) conformational transition. The peptide solubility limited the range of solvent polarity (reflected by the dielectric constant) which could be investigated. The dielectric constant (ε) is calculated as the average of the values for the two miscible solvents according to their relative percentage (ε for 2-propanol is 18.3 Debye units). As a control, a single solvent, trifluoroethanol (TFE), whose ε is equivalent to that of 80% 2-propanol in H_2O, yielded a similar helical content for repeat III (i.e. ca. 45%) as the mixture.

Taking into account the errors bars associated with the helical and β-sheet contents (Fig. 2), it can be safely inferred that the conformational changes exhibited by repeats III and IV are significantly different. This is not the case for repeats I and II. At this stage, it is worth keeping in mind that the latter share a proline in position 19 whilst this proline in repeat III occurs at position 14 and that repeat IV is devoid of any proline. The broadest polarity-dependent conformational transition is observed with S4L45 from repeat III: between $\varepsilon = 30$ and 66, its helical content shifts from around 50 to 20% whilst its β-sheet content shifts from 5 to 45%. Finally, the scrambled peptide does not show such marked sensitivity towards solvent polarity: within the same ε range, helicity is only reduced from 55% to 45%, random coil content making up the remainder (to 100%) with no indication of β-contribution.

We checked the peptide oligomerization state in CD assays by performing parallel analytical ultracentrifugation. At the lower end of the dielectric constant range used in CD, S4L45 of repeat III is monomeric as judged by the molecular weight determined from a sedimentation curve measured with added salt (Fig. 3). This also applies for repeat II. Without added KCl, the highly positively-charged S4L45s cannot be shielded from electrostatic interactions with the trifluoroacetate counter anions (resulting from HPLC elution) and thus the peptide sedimentation equilibrium is displaced towards lower molecular weight (not shown). By contrast and only in the presence of salt, S4L45(II) forms dimers in the high dielectric constant solvent and its solubility is decreased. Thus, these data support the contention that the differential conformational changes of S4L45s are indeed driven by the medium polarity.

Macroscopic conductances: current-voltage curves and kinetics

In the 'macroscopic' configuration, both relatively high peptide bath concentrations (in the *cis*- or positive-side as a rule) and Montal-Mueller planar lipid bilayers of large area ($5 \cdot 10^{-4}\ cm^2$) are used. After equilibration (≈20–30 mn), superimposable current-voltage (I–V) curves resulting from the activity of many channels or conducting aggregates develop in response to slow voltage-ramps. Taking into account the single-channel conductance and the probability of opening (Brullemans et al. 1994), the number of channels activated for instance by S4L45 of repeat IV (Fig. 4A) is about 10^3at the end of the voltage ramp (130 mV) on curve 1. The period of the triangular voltage waveform is slow enough (≈40–60 s per cycle) to ensure steady-state, as checked by comparison of I–V curves derived from ramps and those reconstructed from responses to voltage pulses of increasing amplitudes.

As shown in Fig. 4A (for repeat IV), the general pattern of I–V curves induced by the present class of peptides is quite reminiscent of the one described for alamethicin, i.e. a steep exponential branch developing above a threshold which is dependent on the peptide bath aqueous concentration (curves 1 and 2). The parameters defined in the 'Materials and Methods' section, Ve and Va-voltage-sensitivity and concentration – dependence, respectively – are illustrated in the figure (part A) and their derivation is explained in the legend. Main differences with alamethicin lie in the higher peptide bath concentration needed to develop these I–V curves (alamethicin being much more hydrophobic than the charged S4L45s) and the tendency of the present peptides to yield more symmetrical curves, with respect to current and voltage origins. In this paper, for the sake of simplicity, the analysis of macroscopic I–V curves is restricted to the positive quadrant.

N-deleted fragments from repeat IV. Figure 4B compares I–V curves displayed by the N-deleted fragments (27-mer and 19-mer) of S4L45 from repeat IV. Both voltage- and concentration-dependences are conserved in the 27-mer fragment when compared to the whole peptide (Fig. 4A and B, Table 3). By contrast, and despite the fact that 19-mer helical peptides are still long enough to span bilayers and induce voltage-dependent current (see e.g. Hall et al. 1984; Duclohier et al. 1989), a further 8-residue deletion abolishes all significant activity (Fig. 4B), even after a large concentration increase. It thus appears that the central charged portion of S4 – the LA**R**IA**R**VL stretch –

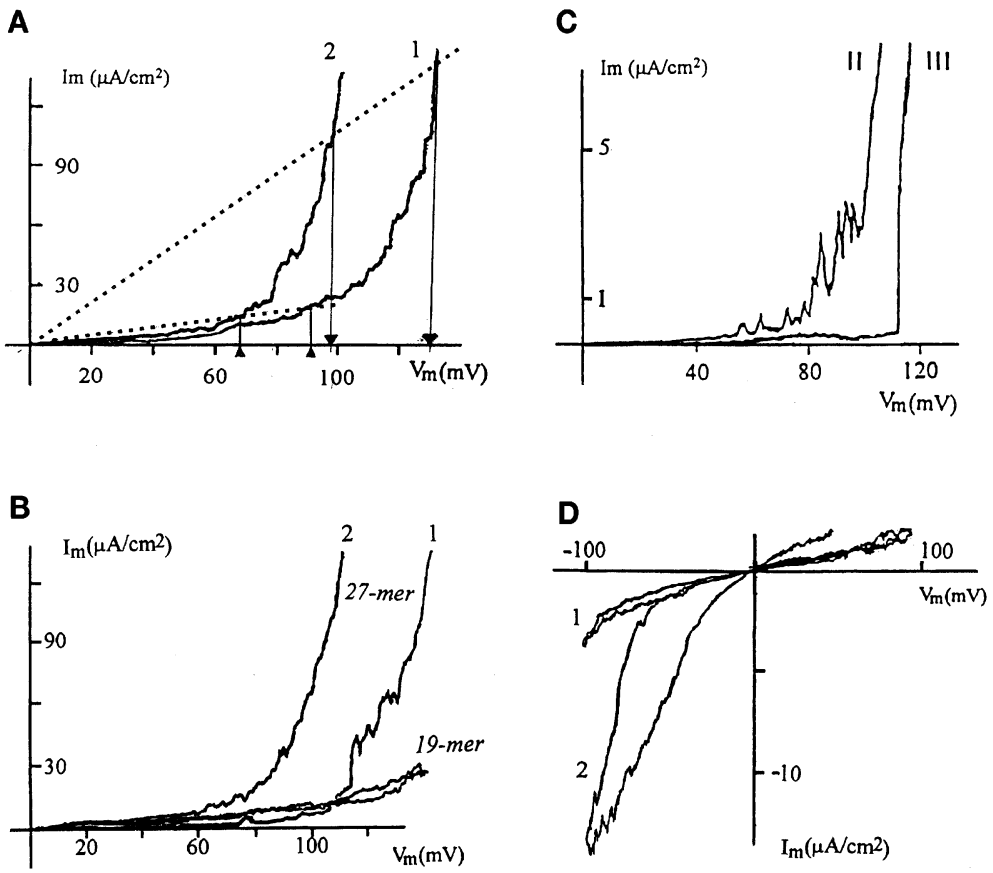

Fig. 4 **A** Macroscopic current-voltage (I–V) curves induced by S4L45 (IV) at 200 (curve 1) and 300 nM (curve 2). Dashed lines indicate slope conductance differing by e^2 to define Ve as half the voltage shift for the exponential branch to reach these conductances (between upward and downward arrows). Concentration dependence is depicted by those arrows pointing in the same direction. **B** I–V curves compared for 27-mer and 19-mer fragments at different peptide concentrations in the bath: 400 nM (curve 1), 600 nM (curve 2) for the 27-mer fragment and 2 μM for the 19-mer fragment. **C**, Comparison of the voltage dependence of proline containing repeats II and III. Peptide bath concentrations are 180 nM for repeat II and 2 μM for repeat III. **D** I–V curves for the scrambled peptide at high bath concentrations (curve 1, 600 μM; curve 3 μM). Same conditions throughout the whole figure: buffered 0.5 M NaCl both sides of neutral POPC/DOPE (7/3) bilayers, room temperature

Table 3 Analysis of the macroscopic conductance data (mean± SEM, 5 experiments per set) from the four eel homologues (*upper part*), fragments of repeat IV (*lower part*), the hskm1 (D4/S4 analogues, and the scrambled peptide. Values for repeats III and IV are in bold

Peptide	Ve	Va	⟨N⟩	Proline position	R^+ & K^+ total number
S4-L45 (I)	8±3	50±7	6	19	7
S4-L45 (II)	9±3	50±8	5–6	19	6
S4-L45 (III)	**6±2**	25±5	4	**14**	**8**
S4-L45 (IV)	**19±4**	90±10	4–5	**none**	**8**
27mer (IV)	19±2	80±10	4–5	none	6
19mer (IV)	∞	–	–	none	4
hskm1 S4(IV) W.T.	**17±2**	ND	–	**none**	8
hskm1 S4(IV) R1457P	**11±2**	ND	–	**13**	7
Scrambled	19±4	ND	ND	7	7

would be essential to detect the transmembrane electric field.

Comparison of I–V curves induced by the homologous voltage sensors. Figure 4C compares macroscopic I–V curves displayed by S4L45s of repeats II and III. Repeat I behaves as its homologue of domain II (Table 3). We selected exponential branches developing within a similar range of applied voltage (100–110 mV) since there was a slight influence of voltage on Ve. For instance in Fig. 4A (S4L45 of repeat IV), on shifting from 130 to 95–100 mV (for reaching the same conductance depicted by the upper dashed line) after a 1.5 fold concentration increase, Ve decreases from 19.2 to 14.5 mV. The averaged value (17 mV) is within the range given for the overall mean resulting from pooling 10 independent experiments (Table 3). As illustrated by the steepnesses of the exponential branches (Fig. 4A and C) and as analyzed in Table 3, voltage-sensitivities (Ve) appear significantly different for repeats III and IV (Ve ≈ 6 vs 19 mV, respectively) whilst they assumed similar intermediate values for repeats I and II (Ve ≈ 8–9 mV). Despite a smaller number of positive charges in S4s of repeats I and II (i.e. 6–7) and an identical number in repeat III as in repeat IV (8 positive charges), their Ve is significantly reduced and thus their voltage-dependence is higher. This is matched by smaller concentration-dependences: the voltage shift of threshold upon an e-fold change in concentration (Va) being 50 mV for both repeats I and II, and 25 mV for repeat III, as opposed to 90 mV for repeat IV. Thus overall, on applying the relation ⟨N⟩ = Va/Ve (see methods), the average sizes of the conducting aggregates are conserved: ⟨N⟩ = 4–6. Note that the current developed by repeat IV is at least one order of magnitude larger than with the other repeats and this simply reflects the 'safety factor' we had to respect: the high voltage sensitivity displayed by repeats I, II and

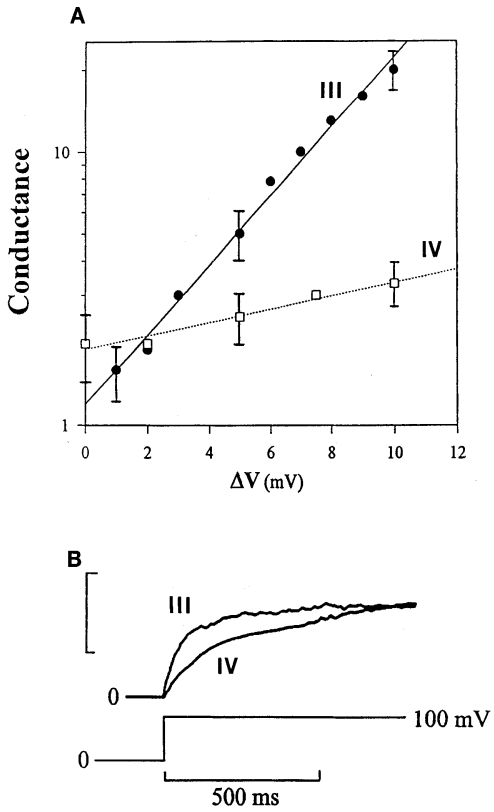

Fig. 5 **A** Semi-log plot of macroscopic conductance versus voltage increments after threshold for repeats III and IV. To facilitate comparison, conductances were normalized towards the start of the exponential branch and are given in arbitrary units. Voltage increments resulting in e-fold change in conductance are Ve = 5 and 16 mV for repeats III and IV, respectively. **B** Current kinetics exhibited by the same repeats (III and IV) during a 100 mV voltage step. The peptide concentrations were adjusted so as to yield similar current density. Capacity transients and residual leakage currents were substracted (from negative pulses) and averaged curves were later normalized and smoothed. Time constants are about 75 and 220 (±10%) ms, respectively, for the specified step amplitude. Vertical scale bar indicates 10 μA/cm^2 for repeat IV

III precludes attaining large current density due to increased risks of dielectric breakdown (bilayer rupture).

The upper part of Table 3 shows that the intrinsic voltage-sensitivities (Ve) of the four homologous eel S4L45s are better correlated to the presence and position of a single proline than to the number of positive residues. Indeed, whereas repeat IV devoid of Pro displays by far the lowest voltage-sensitivity, the first two repeats sharing Pro19 present a similar Ve and repeat III (Pro14) has the highest voltage-sensitivity. This influence of Pro upon voltage sensitivity is confirmed and more directly probed with two S4 segments of domain IV from the human skeletal muscle sodium channel: the wild type S4 segment and an analogue where the fourth arginine (corresponding to position 1457 in the intact skm1 sequence, George et al. 1992) was substituted by a proline. The analysis of voltage sensitivity yields on average 17 vs. 11 mV, respectively, despite the loss of one arginine (Table 3).

As for the scrambled peptide, it develops some voltage-dependent branch but in the negative quadrant (Fig. 4D) presumably due to the clustering of positively-charged residues near the C-terminus rather than on the other half as in S4s (see Hall et al. 1984, for a parallel with alamethicin derivatives). Leak conductance is also significantly higher and, despite bearing a proline residue (but close to the N-terminus), its Ve is comparable to the least voltage-sensitive homologue (i.e. repeat IV).

The markedly different voltage sensitivities associated with eel repeats III and IV are further highlighted in Fig. 5A, on a semi-log plot of macroscopic conductance versus voltage. Here, Ve = 5 and 16 mV for repeats III and IV, respectively. This translates into modulated kinetics of the macroscopic current in response to voltage steps (Fig. 5B): repeat III rises earlier than repeat IV.

Discussion

In this study we show that synthetic peptides derived from the four voltage-sensors of the eel sodium channel display voltage-sensitivity which appears correlated to the presence and position of a single proline residue. This finding is corrobated by macroscopic experiments on wild type and R → P substituted S4s of the human skeletal muscle sodium channel (domain IV), albeit with a smaller difference in Ve. A similar mutation affecting the first arginine of that segment (R1448P) results in a rare but severe form of *Paramyotonia congenita* (Wang et al. 1995). This functional modulation due to the position of Pro associated with a broad polarity-dependent conformational switching (especially in repeat III) is an intriguing outcome which is suggestive for gating mechanisms. The low voltage-sensitivity of the scrambled peptide despite its proline, together with its relative stable conformation towards solvent polarity and its greater tendency to induce background voltage-independent conductance near 0 mV, set this peptide apart from the four homologous S4L45s. In the remainder of this Discussion, we shall concentrate on the behavior of S4L45s in macroscopic conductance and conformational assays with the view of drawing possible implications for channel gating.

Since voltage-dependence is preserved in the 27-mer of S4L45 (IV) despite the loss of two arginines near the N-terminus and since the 19-mer fragment is inactive, the central portion of S4 with the third and fourth arginines nearly corresponding to S4h of Guy and Conti (1990) would appear the most essential part of the gating machinery, at least at this level of 'isolated peptide investigation'. An eel D4/S4 (i.e. S4 segment from domain IV), lacking the first three residues (the TLF motif) and most of the L45 linker (see Table 1: T peptide) as compared to the sequences studied here, was already shown to induce exponential I–V curves (Tosteson et al. 1989). Its voltage-dependent conductance was Ve ≈ 10 mV for a threshold about 20 mV less depolarized than curve 2 of Fig. 4A. Taking into account the slight Ve modulation by voltage (see above

'Comparison of I–V curves …'), this is equivalent to values found with our 29-mer. Thus, deleting the 9 residues at C-terminus does not seem to have the drastic effect of the second N-deletion encompassing the third and fourth arginines. Note that the most sensitive Pro position is close to R4 already found to possibly be the most important voltage sensing arginine (Kontis et al. 1997). In the substituted hskm1 D4/S4, the substituted arginine was also the fourth one in the peptide sequence and the same number of arginines (two) have been shown by Yang et al. (1996) to move entirely across the field. Here, we further show that macroscopic conductances induced by S4L45 of repeats I to III were much more voltage-dependent than the peptide initially tested (S4L45 of repeat IV). Thus, Pro seems to overcompensate the smaller number of charged residues shown in site-directed mutagenesis to be essential as voltage-sensors in the expressed sodium channel (Stühmer et al. 1989). The most voltage-sensitive S4L45 is from repeat III (Ve = 4–6 mV, as in the intact in situ channel) with only four arginines and a lysine ahead of Pro14, the latter being also shared by the unrelated alamethicin which, coincidentally, has a quite similar Ve (Gordon and Haydon 1975).

Applying the equation $q = \langle N \rangle z\, d = (RT/F)/Ve$, where $z\, d$ is the product of the peptide monomer 'mobile' charge and the fraction of voltage drop or membrane thickness it traverses (others symbols have their usual definitions), yields a gating charge of 10 to 3 for repeats III and IV, respectively the highest and lowest voltage-sensitive elements. In the event that the four different homologuous voltage sensors would equally and simultaneously contribute in the context of the intact channel, this would represent an average gating charge of 7 (i.e. ≈29/4). This value is quite similar to the ones (6–8, occurring in three shots) derived from gating current analysis of rat brain II sodium channels expressed in *Xenopus* oocytes (Conti and Stühmer 1989) but smaller than recent estimates (i.e.: 12) by Hirschberg et al. (1995), extending the analysis of the single-channel activation curve towards very small open probability.

Still at the whole channel level, Pro additions or deletions in S4s of rat brain sodium channel II expressed in oocytes were not found to significantly affect activation but rather altered their mode of inactivation (Moran et al. 1994). In another study, on Kv1.1 K^+ channel, a proline introduced in any one of the four S4s reduced the slope of the activation curve whilst if Pro was added to two subunits, the latter were excluded from pore formation (Hurst et al. 1995). This is rather challenging, since prolines are largely conserved in the first three domains of sodium channels. In view of these contrasted data and also of the correlated structural and functional modulations reported here, it might prove worthwhile to carry out an investigation on the effects of Pro analogues modulating *cis-trans* isomerization (see e.g. Yaron and Naider 1993) upon channel properties.

As reported above, the investigation of the conformational contents of the four homologues as a function of dielectric constant reveals a helical → extended (β-sheet + random coil) transition. It was previously shown that this transition is most pronounced for the L45 moiety, at least in repeat IV (Helluin et al. 1996) which has been confirmed recently to complete the inactivation 'receptor' (McPhee et al. 1998). Since S4L45s might experience different polarity environments in the open and closed states, we suggest that a similar process could occur in the context of the channel functioning. Indeed, the fact that the broadest polarity-dependent conformational transition is observed with the most voltage-sensitive peptide (S4L45 from repeat III) might not be fortuitous but could open scope for gating mechanisms. Specifically, we favour for the gating process some unfolding which would leave only two arginines in a protein interior that would still span most of the bilayer. Alongside the translocation of otherwise unperturbed S4 across short protein "canaliculi" (Yang et al. 1996), S4 helix-coil transition for gating constitutes an alternative mentioned in Sigworth's review (1993). This scheme is also reminiscent of the model by Guy and Conti (1990) and has already been proposed in the literature (Benndorf 1989; Leuchtag 1994). The quite small free-energy differences resulting from substantial S3–S4 linker alterations (*Shab-Shaw* → *Shaker* K^+ channels, see Mathur et al. 1997) somewhat preclude large outward movement of S4s but are still consistent with local secondary structure changes of the kind hypothesized in the present study and similar to the proposal of a helix-to-loop rearrangement of S4s (Aggarwal and MacKinnon 1996).

Whether or not the same sequence of voltage-sensitivity and hence of kinetics as reported here with isolated reconstituted voltage-sensors -S4 (III) would initiate gating, followed by its homologous from domains I and II whilst S4 (IV) would complete the process leading to channel opening- would still hold in the in situ whole channel remains a matter of investigation. It is possible that the functional and conformational differences reported here could be 'softened' by domain interactions or different degrees of co-operativity in activation kinetics (Keynes and Elinder 1998). Preliminary investigations of voltage sensitivity in mixed reconstitution assays (repeats III + IV) into planar lipid bilayers suggest molecular co-operativity. It is however interesting to note that recent cysteine mutagenesis studies support some degree of asymmetry (or of specialized function for the four domains) in sodium channels with respect to gating (Kontis et al. 1997) and the pore region as well (Bénitah et al. 1997).

The present study of isolated voltage sensors interacting with planar lipid bilayers does not imply that they are in immediate proximity within the intact channel since four molecules of a relatively large spider toxin can bind simultaneously to externally accessible sites of S4s, at least in the drk1 potassium channel (Swartz and MacKinnon 1997). However, S4s environment in the intact channel is partly hydrophobic and only a few negatively-charged residues (mainly at either end of S2 and S3 segments) evenly distributed between the four domains can form ion pairs with hardly half the arginines and lysines. Thus, the gating mechanism we proposed here remains plausible for the sodium channel. We are now addressing the voltage sensitivity of S3–S4 fragments and S3 (S2 is inactive in pla-

nar lipid bilayers) and implementing time-resolved CD and fluorescence spectroscopies in an attempt to more directly probe any voltage-driven conformational changes.

Acknowledgements We thank the C. E. B. (Mont-Saint-Aignan, Fr) for peptide synthesis and purification facilities, and Dr. J.-C. Blais (Laboratoire de Chimie Structurale Organique et Biologique, Paris VI Université) for MALDI mass spectroscopy. We are greatly indebed to Dr J. D. Lear (Department of Biochemistry and Biophysics, University of Pennsylvania School of Medicine, Philadelphia) for his help and expertise in the analytical centrifugation assays, and to Dr M. Beyermann (Institute of Molecular Pharmacology, Free University of Berlin, Germany) for the preparation of hskm1 D4/S4 (W. T.). We also thank Dr. I. Vodyanoy and Dr. P. Cosette for critical reading of the manuscript. Supported by GdR 1153 CNRS "Peptides et Protéines Amphipathiques".

References

Aggarwal SK, MacKinnon R (1996) Contribution of the S4 segment to gating charge in the *Shaker* K^+ channel. Neuron 16: 1169–1177

Atherton E, Sheppard RC (1989) Solid phase peptide synthesis: a pratical approach. IRL Press, Oxford

Auld VJ, Goldin AL, Krafte DS, Catterall WA, Lester HA, Davidson N, Dunn RJ (1990) A neutral amino acid change in segment IIS4 dramatically alters the gating properties of the voltage-dependent sodium channel. Proc Natl Acad Sci USA 87: 323–327

Barlow DJ, Thornton JM (1988) Helix geometry in proteins. J Mol Biol 201: 601–619

Barsukov IL, Nolde DE, Lomize AL, Arseniev AS (1992) Three-dimensional structure of proteolytic fragment 163–231 of bacteriopsin determined from nuclear magnetic resonance data in solution. Eur J Biochem 206: 665–672

Bénitah JP, Ranjan R, Yamagishi T, Janecki M, Tomaselli GF, Marban E (1997) Molecular motions within the pore of voltage-dependent sodium channels. Biophys J 73: 603–613

Benndorf K (1989) A reinterpretation of Na channel gating and permeation in terms of a phase transition between a transmembrane S4 a-helix and a channel-helix. Eur Biophys J 17: 257–271

Brahms S, Brahms J (1980) Determination of protein secondary structure in solution by vacuum ultraviolet circular dichroism. J Mol Biol 138: 149–178

Braswell E (1987) Polyelectrolyte charge corrected molecular weight and effective charge by sedimentation. Biophys J 51: 273–281

Brooks JS, Soneson KK, Hensley P (1993) Development and use of a mac based data analysis package for equilibrium sedimentation data from the analytical ultracentrifuge. Biophys J 64: a244

Brullemans M, Helluin O, Dugast J-Y, Molle G, Duclohier H (1994) Implication of segment S45 in the permeation pathway of voltage-dependent sodium channels. Eur Biophys J 23: 39–49

Cha A, Bezanilla F (1997) Characterizing voltage-dependent conformational changes in the shaker K^+ channel with fluorescence. Neuron 19: 1127–1140

Chang CT, Wu CSC, Yang JT (1978) Circular dichroic analysis of protein conformation: inclusion of the β-turns. Anal Biochem 91: 13–31

Conti F, Stühmer W (1989) Quantal charge redistributions accompanying the structural transitions of sodium channels. Eur Biophys J 17: 53–59

DeGrado WF, Wasserman ZR, Lear JD (1989) Potein design, a minimalist approach. Science 243: 622–628

Duclohier H, Molle G, Spach G (1989) The influence of trichorzianin C-terminal residues on the ion channel conductance in lipid bilayers. Biochim Biophys Acta 987: 133–136

Durell SR, Guy HR (1992) Atomic scale structure and functional models of voltage-gated potassium channels. Biophys J 62: 238–250

Durell SR, Guy HR (1996) Structural model of the outer vestibule and selectivity filter of the *Shaker* voltage-gated K^+ channel. Neuropharmacology 35: 761–773

Elmer LW, O'Brien BJ, Nutter YJ, Angelides KJ (1985) Physicochemical characterization of the a-peptide of the sodium channel from rat brain. Biochemistry 24: 8128–8137

Favre I, Moczydlowski E, Schild L (1996) On the structural basis for ionic selectivity among Na^+, K^+, and Ca^{2+} in the voltage-gated sodium channel. Biophys J 71: 3110–3125

Furst A (1997) The XL-I analytical ultracentrifuge with Rayleigh interference optics. Eur Biophys J 35: 307–310

George AI Jr, Komisarof J, Kallen RG, Barchi RL (1992) Primary structure of the adult human skeletal muscle voltage-dependent sodium channel. Ann Neurol 31: 131–137

Gordon LGM, Haydon DA (1976) Potential-dependent conductances in lipid membranes containing alamethicin. Phil Trans Roy Soc Lond B 270: 433–447

Greenblatt R, Blatt Y, Montal M (1985) The structure of the voltage-sensitive sodium channel. Inferences derived from computer-aided analysis of the *Electrophorus electricus* channel primary structure. FEBS Lett 193: 125–134

Guy HR, Conti F (1990) Pursuing the structure and fonction of voltage-gated channels. Trends Neurosci 13: 201–206

Guy HR, Seetharamulu P (1986) Molecular model of the action potentiel sodium channel. Proc Natl Acad Sci USA 83: 508–512

Hall JE, Vodyanoy I, Balasubramanian TM, Marshall GR (1984) Alamethicin: a rich model for channel behaviour. Biophys J 45: 233–247

Helluin O, Breed J, Duclohier H (1996) Polarity-dependent switching of a peptide mimicking the S4–S5 linker of the voltage-sensitive sodium channel. Biochim Biophys Acta 1279: 1–4

Hirschberg B, Rovner A, Lieberman M, Patlak J (1995) Transfer of twelve charges is needed to open skeletal muscle Na channels. J Gen Physiol 106: 1053–1068

Hurst RS, North RA, Adelman JP (1995) Potassium channel assembly from concatenated subunits: effects of proline substitutions in S4 segments. Receptors and Channels 3: 263–272

Kahn TW, Engelman DM (1992) Bacteriorhodopsin can be refolded from two independently stable transmembrane helices and the complementary five-helix fragment. Biochemistry 31: 6144–6151

Kerr ID, Sansom MSP (1997) The pore-lining region of *Shaker* oltage-gated potassium channels: comparison of β-barrel and α-helix bundle models. Biophys J 73: 581–602

Keynes RD, Elinder F (1998) Modelling the activation, opening, inactivation and reopening of the voltage-gated sodium channel. Proc R Soc B 265: 263–270

Kontis KJ, Rounaghi A, Goldin AL (1997) Sodium channel activation gating is affected by substitutions of voltage sensor positive charges in all four domains. J Gen Physiol 110: 391–401

Kreusch A, Pfaffinger P, Stevens CF, Coe S (1998) The crystal structure of the putative ion-conducting pathway formed by the inner vestibule of *Shaker* potassium channel. Biophys J 74: A127

Laue T, Shaw BD, Ridgeway TM, Pelletier SL (1992) Computer-aided interpretation of analytical sedimentation data for proteins. In: Harding SE, Rowe AJ, Horton JC (eds) Analytical Ultracentrifugation in Biochemistry and Polymer Science. The Royal Society of Chemistry, Cambridge, UK, pp 90–125

Leuchtag HR (1994) Long-range interactions, voltage sensitivity, and ion conduction in S4 segments of excitable channels. Biophys J 66: 217–224

Li M, Unwin N, Stauffer KA, Jan Y-N, Jan LY (1994) Images of purified *Shaker* potassium channels. Current Biol 4: 110–115

Lipkind GM, Fozzard HA (1994) A structural model of the tetrodotoxin and saxitoxin binding site of the Na^+ channel. Biophys J 66: 1–13

Logothetis DE, Movahedi S, Satler C, Lindpainter K, Nadal-Ginard B (1992) Incremental reductions of positive charge within the S4 region of a voltage-gated K^+ channel result in a corresponding decrease in gating charge. Neuron 2: 531–540

Lopez GA, Jan Y-N, Jan LY (1991) Hydrophobic substitution mutations in the S4 sequence alter voltage-dependent gating in *Shaker* K^+ channels. Neuron 2: 327–336

Mannuzzu LM, Maronne MM, Isacoff EY (1996) Direct physical measure of conformational rearrangement underlying potassium channel gating. Science 271: 213–216

Marsh D (1996) Peptide models for membrane channels. Biochem J 315: 345–361

Mathur R, Zheng J, Yan Y, Sigworth FJ (1997) Role of the S3–S4 linker in *Shaker* potassium channel activation. J Gen Physiol 109: 191–199

McPhee J, Ragsdale DS, Scheuer T, Catterall WA (1998) A critical role for the S4–S5 intracellular loop in domain IV of the sodium channel a-subunit in fast inactivation. J Biol Chem 273: 1121–1129

Montal M (1995) Design of molecular function: channels of communication. Annu Rev Biophys Biomol Struct 24: 31–57

Montal M (1996) Protein folds in channel structure. Current Opinion in Struct Biol 6: 499–510

Montal M, Mueller P (1972) Formation of bimolecular membranes from lipid monolayers and a study of their electrical properties. Proc Natl Acad Sci USA 69: 3561–3566

Moran O, Gheri A, Zegarra-Moran O, Imoto K, Conti F (1994) Proline mutations on the S4 segment of rat brain sodium channel II. Biochem Biophys Res Comm 202: 1438–1444

Noda M, Shimuzu S, Tanabe T, Takai T, Kayano T, Ikeda T, Takahashi H, Nakayama H, Kanaoka Y, Minamino N, Kangawa K, Matsuo H, Raftery MA, Hirose T, Inayama S, Hayashida H, Miyata T, Numa S (1984) Primary structure of *Electrophorus electricus* sodium channel deduced from cDNA sequence. Nature 312: 121–127

Oiki S, Danho W, Montal M (1988) Channel protein engineering: synthetic 22-mer peptide from the primary structure of the voltage-sensitive sodium channel forms ionic channels in lipid bilayers. Proc Natl Acad Sci USA 85: 2393–2397

Perozo E, Santacruz-Toloza L, Stefani E, Bezanilla F, Papazian DM (1994) S4 mutations alter gating currents of shaker K^+ channels. Biophys J 66: 345–354

Planells-Cases R, Ferrer-Monteil AV, Patten CD, Montal M (1995) Mutation of conserved negatively charged residues in the S2 and S3 transmembrane segments of a mammalian K^+ channel selectively modulates channel gating. Proc Natl Acad Sci USA 92: 9422–9426

Sansom MSP (1991) The biophysics of peptide models of ion channels. Prog Biophys Mol Biol 55: 139–235

Seoh S-A, Sigg D, Papazian DM, Bezanilla F (1996) Voltage-sensing residues in the S2 and S4 segments of the *Shaker* K^+ channels. Neuron 16: 1159–1167

Sigworth FJ (1993) Voltage gating of ion channels. Q Rev Biophys 27: 1–40

Spencer RH, Sokolov Y, Li H, Takenaka B, Milici AJ, Aiyar J, Nguyen A, Park H, Jap BK, Hall JE, Gutman GA, Chandy KG (1997) Purification, visualization, and biophysical characterization of Kv1.3 tetramers. J Biol Chem 272: 2389–2395

Stühmer W (1991) Structure-function studies of voltage-gated ion channels. Annu Rev Biophys Chem 20: 65–78

Stühmer W, Conti F, Suzuki H, Wang X, Noda M, Yahagi N, Kuo H, Numa S (1989) Structural parts involved in activation and inactivation of the sodium channel. Nature 339: 597–603

Swartz KJ, MacKinnon R (1997) Mapping the receptor site for hanatoxin, a gating modifier of voltage-dependent K^+ channels. Neuron 18: 675–682

Tang C-Y, Papazian DM (1997) Transfer of voltage independence from a rat olfactory channel to the *Drosophila* ether-a-go-go K^+ channel. J Gen Physiol 109: 301–311

Tiwari-Woodruff SK, Schulteis CT, Mock AF, Papazian DM (1997) Electrostatic interactions between transmembrane segments mediate folding of *Shaker* K^+ channel subunits. Biophys J 72: 1489–500

Tosteson MT, Auld DS, Tosteson DC (1989) Voltage-gated channels formed in lipid bilayers by a positively charged segment of the Na-channel polypeptide. Proc Natl Acad Sci USA 86: 707–710

Wang J, Dubowitz V, Lehmann-Horn F, Ricker K, Patcek L, Hoffman EP (1995) In vivo sodium channel structure/function studies: consecutive Arg 1448 changes to Cys, His, and Pro at the extracellular surface of IVS4. Soc Gen Physiol Ser 50: 77–88

Yang N, George AL Jr, Horn R (1996) Molecular basis of charge movement in voltage-gated sodium channels. Neuron 16: 113–122

Yaron A, Naider F (1993) Proline-dependent structural and biological properties of peptides and proteins. Crit Rev Biochem Molec Biol 28: 31–81